Energy and Buildings 43 (2011) 2727–2736

Contents lists available at ScienceDirect

Energy and Buildings

journal homepage: www.elsevier.com/locate/enbuild

Flow generated by a thermal plume in a cooled-ceiling system

Luis P. Thomas[a,*], Beatriz M. Marino[a], Ramón Tovar[b], José A. Castillo[b]

[a] GFGA, Facultad de Ciencias Exactas, Universidad Nacional del Centro de la Prov. de Buenos Aires, Pinto 399, B 7000 GHG Tandil, Argentina
[b] Centro de Investigación en Energía, Universidad Nacional Autónoma de México Priv. Xochicalco s/n, Col. Centro, Temixco, Morelos, Mexico

ARTICLE INFO

Article history:
Received 17 January 2011
Received in revised form 13 June 2011
Accepted 21 June 2011

Keywords:
Cooled ceiling
Thermal plumes
Indoor comfort

ABSTRACT

The transient and steady states of the flow generated by a heat source inside a closed room provided with a cooled-ceiling system at constant temperature are experimentally studied. During the transient regime the plume generated by the source interacts with the ambient fluid and, after it reaches the top contour, spreads under the latter giving place to the formation of a horizontal thermal front that eventually descends affecting the whole room. It is found that the formation and velocity of the descending front are determined by the *filling-box* model in an insulated space but with a smaller temperature difference between both sides of the front. The steady state is established when the heat supplied by the source is completely absorbed by the ceiling allowing a convective process to take place characterized by a turbulent flow in the major part of the room and by a thermal boundary layer developed below the ceiling, where vortexes and little plumes form, the detection of which is allowed by the application of synthetic schlieren technique. Analogies with the results obtained in the classical Rayleigh–Benard experiments allow an insight of the mechanisms of heat transfer in order to improve the indoor comfort in buildings under similar conditions to those discussed here.

1. Introduction

Since the quality of the inner spaces is an increasingly important part of the environment, modern designers make imaginative use of the architectural resources to create well-lit and attractive interiors. In an attempt to optimize the quality indoors in terms of comfort and temperature particularly, there has been a rising trend towards the use of mechanical devices with undesirable energy implications and high carbon dioxide emissions.

Sources of buoyancy, such as occupants, domestic appliances, computers, etc. which are within the rooms and have smaller sizes than the overall space, may generate significant heat gains inside buildings. These sources tend to be isolated and produce buoyant plumes that rise above them. The warm air accumulates near the ceiling and a stable stratification is established within each room of the building. Different vertical stratifications generated in adjacent spaces with dissimilar heat loads can drive flows through the openings in the dividing walls [1]. As a result there has been a reawakened interest in taking advantage of natural ventilation to provide high-quality indoor ambient, in commercial and industrial buildings which are subject to increasingly strict environmental and health regulations concerning air quality, and in houses. Natural ventilation uses the available free resources of the wind and thermal energy that results of solar and incidental heating of the building. The main factors controlling indoor air quality are the air movement responsible for transporting both heat and pollutants and the building fabric, which influences the perceived temperature by radiative effects and by heat exchanges with the air. A number of experiments and theoretical studies have examined the natural ventilation of an enclosure. The majority of these studies have concentrated on ventilation flows which are solely driven by either “the buoyancy force associated with the temperature difference between the fluid inside the enclosure and that of its surroundings” or “the wind” (see [2,3] and references therein).

Also heating, ventilating and air-conditioning (HVAC) systems provide high indoor air quality and thermal comfort although they are the largest energy consumers in constructions. These systems are particularly important in the design of large industrial and office buildings such as skyscrapers and in marine environments such as aquariums, where safe and healthy building conditions are regulated with temperature and humidity, as well as fresh air from outdoors. One of the HVAC systems that attracted attention for its potential for energy savings while providing high indoor air quality and thermal comfort is a combined cooled-ceiling (CC) and displacement ventilation (DV) system. The CC system removes heat from the heat sources directly by radiation and indirectly by convection, with minimum possible disturbances to the stratified airflow. The most widely used are water-cooled radiant panels built in dropped ceilings. In this case, cooled-water flows through metal tubes connected with metal-sheet panels, remove the heat

* Corresponding author.
E-mail address: lthomas@exa.unicen.edu.ar (L.P. Thomas).

0378-7788/$ – see front matter © 2011 Elsevier B.V. All rights reserved.
doi:10.1016/j.enbuild.2011.06.033

Nomenclature

P	power supplied
T	temperature
Z	vertical coordinate
Q	heat flux
ρ	density
V	volume
c_p	specific heat
t	time
τ	characteristic time
σ	standard deviation
Ra	Rayleigh number
Pr	Prandtl number
Re	Reynolds number
Nu	Nusselt number
α	diffusivity
β	thermal expansion coefficient
λ	thermal conductivity
ν	kinematic viscosity
g	acceleration of gravity
L	distance
U	velocity
f_c	characteristic frequency
T'	amplitude of temperature fluctuations

collected by the panels maintained at an approximately constant temperature. Different ways exist in order to maintain constant the temperature of the panels that dissipate the absorbed heat [4–6] and humidity in a range of acceptable values [7]. However, the comfort conditions achieved and the efficiency of the system are mainly related to the cooling of the indoor air by radiation and convection [8,9], together with the stratification in the room [10]. This type of system may eventually be integrated to other passive systems [11,12]. Because of the fast dynamic response and capability to use plenum above the cooling panels for building service systems, the water-cooled radiant panels seem to be most suitable and popular for combination with DV. When cooled ceilings are properly designed, operational costs and more usable building space can also be achieved while latent loads and pollutants have to be removed by an additional ventilation system.

In order to recognize the main characteristic of the resultant flow in a building, we focus our attention in a simplified configuration as that of an insulated room with a unique heat source located on the floor and a CC system. To our knowledge, the convective process generated by the combination of one or more plumes in an insulated room [13–17] with a cooled-ceiling system has not been dealt with yet and consequently the understanding of the results involved becomes the goal of this paper. The transient and steady regimes of the flow generated are analyzed by means of experiments by applying the methodology of small-scale modeling using water as the working fluid instead of air as proposed by Linden et al. [18] and Baker and Linden [19]. To visualize and quantify the temperature variations, synthetic schlieren technique is used while temperature at different heights is measured by means of a thermocouples array. We found that the dynamics of the flow is initially similar to that developed when the roof is insulated, which is described by the classical filling-box model developed by Baines and Turner [14]. The plume of smaller density than the surroundings, originated by a source of small size, ascends to the ceiling under which it spreads forming a horizontal thermal front that eventually descends to the floor. The fluid filling the room transmits heat from the source to upper boundary by means of a particular convective process that includes the formation of an unstable boundary layer below the ceiling in which strong fluctuations are detected, thus helping the cooled-ceiling system to achieve the indoor comfort efficiently.

After presenting the experimental setup and methodology, the transient and steady regimes are described. A comparison with the thermally driven flow under the conditions imposed in the well-known Rayleigh–Benard experiments (see for example [20]) allows the validation of the results found and the explanation of the heat transfer process observed. Finally the conclusions are given.

2. Experimental set-up description

The laboratory physical model depicted in Fig. 1 consists of a rectangular 0.60 m long, 0.20 m wide and 0.25 m deep tank with transparent acrylic walls, filled with water initially at uniform ambient temperature. On the bottom center there is a cylindrical electric heater (0.10 m long, 0.014 m diameter) with an electric nominal power $P = 100$ W. The input power is regulated in the range 10–90 W with a *Variac*, thus heating the water by convection as described in the next section. The changes of the heat flow during an experiment may change the dissipation of the heater and its temperature and, consequently, also its internal resistance and the current in the feeding circuit, implying a change of the power supplied. As a result, it is detected that power varies no more than a 4% during each experiment.

The upper contour works as a heat-exchanger and consists of a copper plate of thickness 0.005 m that is soldered to an array of two series of five copper tubes of 0.01 m diameter, connected with their entrances and exits at opposite ends. A *NESLAB* refrigerated bath controls the temperature of the fluid that circulates in the tubes. A neoprene layer of thickness 0.02 m covers the connecting tubes and the roof to thermally insulate the critical part of the system. The temperatures of the copper plate, the heater, the fluid and ambient are measured at intervals of 5 s with a T-type thermocouples net connected to an *Agilent* 34970A device. Ten thermocouples were arranged on a rod separated 0.023 m from each other inside the box. For comparison, one series of experiments was also performed in a filling-box configuration using an acrylic plate of 0.02 m thick as upper insulated contour instead of the heat-exchanger.

A video-camera *Basler* A102k with a 1392×1040 pixels resolution was employed to register the experiments taking one image every 5 s initially and every 10 min after 1 h from the beginning for about 12 h. To minimize the influence of the heat losses, the initial temperature of the fluid and the heat exchanger are chosen so that the temperature estimated for the steady state is approximately the same as the ambient temperature. After the temperature of the NESLAB bath is fixed equal to the ambient's, water is forced to circulate from the lower part of the model to the superior one by means of a small pump for 30 min. Once the thermal homogenization of the fluid finishes and the pump is disconnected, a reference image of the initial distribution of the light intensity is obtained averaging

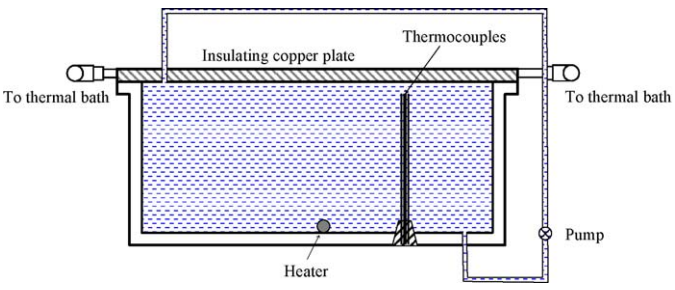

Fig. 1. Schematic of the laboratory physical model.

a sequence of images of this situation. The experiment starts when the heater is turned on.

Synthetic schlieren diagnostic [21] is applied to visualize the evolution of the flow and estimate the vertical and horizontal components of the density, or temperature, gradient. A fluorescent strip lights and a light-diffusing screen located 0.40 m behind the tank provide nearly uniform back-lighting. The beams of light generated by a diffuse light source pass through a mask and the tank forming small angles to the horizontal, and are captured by the video camera located at 5.20 m from the screen. An acetate sheet with small white circular spots of 1 mm diameter randomly distributed on a black background is used as a mask. During each experiment, the variations of the fluid temperature give place to small changes in the refraction index gradient causing the deflection of the light beams. *DigiFlow* software [22] allows the images to be processed easily obtaining qualitative information online. Quantitative results are obtained with an additional processing in which the light intensity variations with respect to the reference image are detected and converted to changes of the vertical and horizontal density gradients.

The heat loss due to conduction through the walls of the model was determined by performing the usual filling-box experiments using an insulated roof. Thus, this loss from the cooled-ceiling is estimated to be 2 W for a difference of 1 °C with the laboratory temperature. In addition, the maximum energy loss by radiation is found to be 0.3 W. Therefore, adding the conductive and radiative losses the energy by time unit absorbed by the exchanger can be up to 0.7 W smaller than the power supplied by the heater.

3. Results

3.1. The transient regime

Two sequences of processed images showing the evolution of the flow generated for different times are presented in Fig. 2. In both cases, the temperature of the upper contours is initially equal to ambient one. The images on the left correspond to the filling-box case with an insulated top contour while those on the right correspond to a CC system model, for similar power supply to each heater (black circle in the center of the floor). The constant size of the lower part of the plume suggests a laminar flow near the heater. The instabilities develop far from the source in the form of vortexes indicating a more turbulent flow and a major convective mixing with the consequent increase of the plume size. In Fig. 2b the lighter fluid reaches the top plate and in Fig. 2c it spreads under it until it reaches the sidewalls. The continuous arrival of warm fluid by means of the plume results in the formation of a sharp horizontal interface (Fig. 2d) that descends progressively (Fig. 2e).

The comparison between both sequences of images indicates that the developed flows are qualitatively similar, even for the formation of a warmer layer below the upper contour and the thermal front descending at the same velocity in both cases. The time for the front to reach the bottom may be calculated by applying the classical filling box model [1,2,14]. However, the difference of intensity observed between left and right images in Fig. 2d and e suggests that the thermal front is weaker in the CC case. This difference is more notorious when the temperature gradient is estimated by means of synthetic schlieren. Fig. 3 shows, in false color, the distribution of the vertical component of the temperature gradient $T^{-1}\partial T/\partial z$ corresponding to the same images shown in Fig. 2. The black zones indicate gradients of negligible magnitude, while cyan and yellow zones correspond to minimum and maximum values, respectively, according to the color scale shown in the lower part of the figure. The zones of significant gradient are associated with the plume and the front in the insulated ceiling case. When the roof is maintained at constant temperature as in the images to the right, the intensity of the thermal front developed is much smaller. Another interesting feature is the presence of zones with important variations of the temperature gradient near the top boundary, about which we will talk about later.

Fig. 4 illustrates the evolution of the temperature since the heater is turned on. In both analyzed situations, the thermocouple located nearest the floor register a constant temperature during the initial phase (first 1000 s approximately) till this position is reached by the thermal front. After that, the temperature rises gradually at all heights maintaining some variation between the upper and lower levels, and differences between both cases start to be more evident. In the insulated box case (Fig. 4a), the mean temperature in the fluid bulk increases linearly with time, consistently with the evolution of an insulated system that receives heat steadily. When the temperature difference with the environment is significant, the measured values deviate from linearity, thus allowing an estimation of the global losses due to conduction as mentioned before. Fig. 4b shows the temperatures measured in the cooled-ceiling model with an enlarged vertical scale. The evolution for the first 1000 s, or even more, is quite similar to the previous case but with a lower rate of temperature increase. At about 15,000 s, the maximum temperature is reached; it is about 2 °C higher than the initial temperature of the fluid. For longer periods of times, important changes in the measurements are not observed suggesting that a steady-state regime is achieved in which all the heat supplied to the fluid is absorbed by the ceiling. In this case the fluid drives the heat supplied by the source mainly by convection. The temperatures of the ceiling and laboratory are also altered during the 11 h that the experiment lasts, but these variations are much smaller than in the fluid.

Neglecting the losses, the energy supplied by the heater is partly employed to increase the internal energy of the fluid and partly absorbed by the heat exchanger. Hence the evolution of the fluid temperature shown in Fig. 4b allows estimating the heat flux $Q = P - \rho V c_p \partial T/\partial t$ in the upper contour, where ρ and c_p are the density and the specific heat of the fluid respectively, while V is the volume of the fluid in the box. The temperature values measured in the whole fluid are averaged, and $\partial T/\partial t$ and Q are calculated; the results are then approximated by the best fit function of the form $T_0 + T_1[1 - \exp(-t/\tau)]$, where T_0, T_1 and τ are constant. As shown in Fig. 5, the heat transfer from the source to the upper contour is initially negligible but afterwards increases quickly, and after a characteristic time $\tau \approx 4360$ s it tends asymptotically to the value supplied by the source. This time is similar to the interval δt spent by the source to heat the fluid until it reaches the temperature difference ΔT between the temperature of the steady-state and the initial one, that is $\delta t = \rho V c_p \Delta T/P = 4180$ s. As noted before, after about $3\tau \approx 15{,}000$ s it may be considered that the system reaches the steady-state regime.

3.2. The steady-state regime

Fig. 6 shows the difference ΔT between the averaged temperature $\langle T \rangle$ at different heights in the fluid and that of the CC, T_{cc}, reached during the steady state for different values of the power supplied to the heater. As expected, the temperature difference increases with the power input while the temperature profiles result very similar presenting a maximum near the upper contour and a minimum on the floor. Fig. 7 shows that the fluid bulk's temperature seems to increase proportionally to the heater power.

In Fig. 4b, the presence of fast fluctuations of 0.5 °C-amplitude is noted in the measurements of temperatures at the levels nearer to the cooled ceiling, which are not registered by the thermocouples in the lowers levels nor in the insulating ceiling case. To quantify

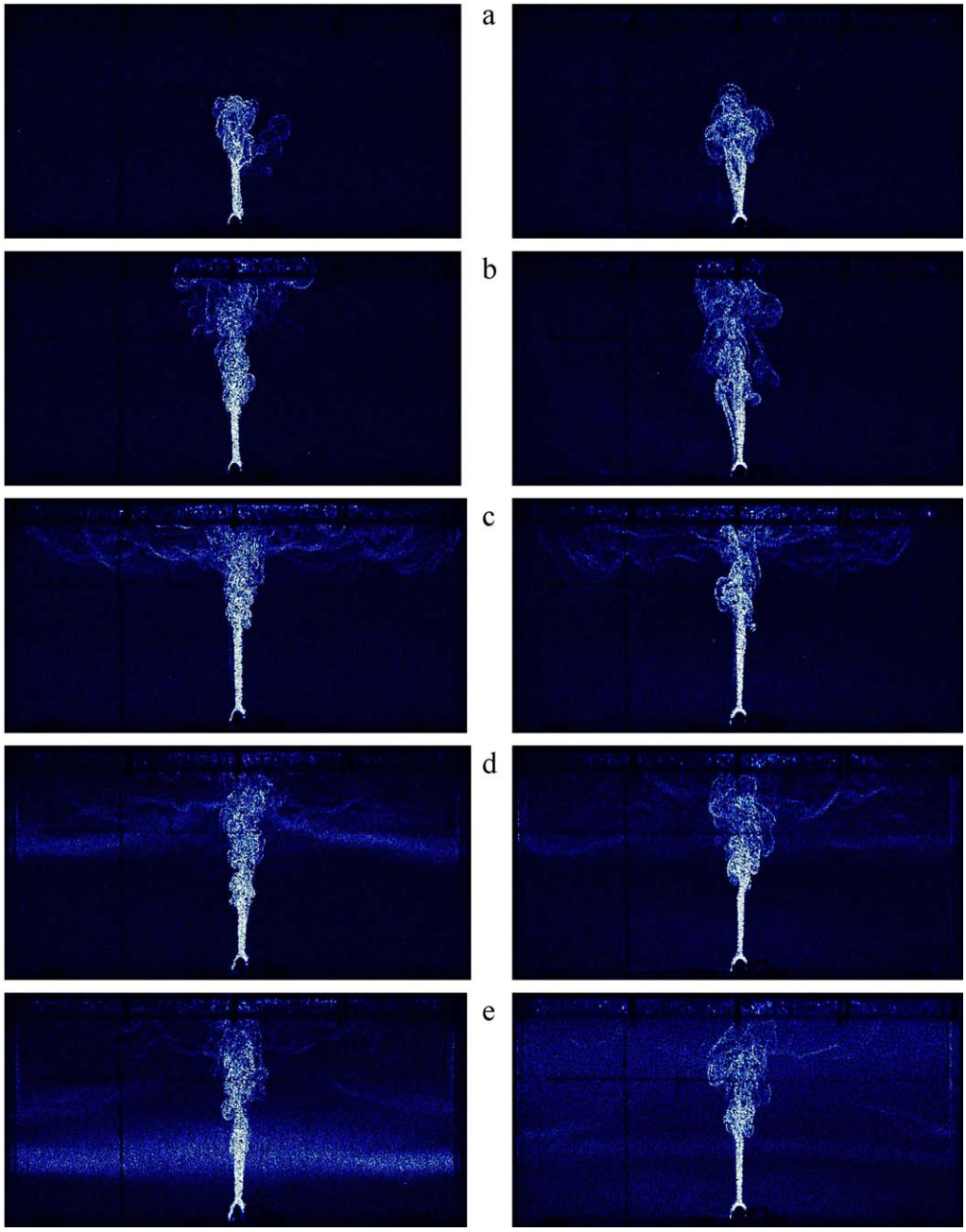

Fig. 2. Images obtained with synthetic schlieren at (a) 20 s, (b) 40 s, (c) 90 s, (d) 250 s and (e) 800 s after the 60 W heater is turn on for the cases in which the upper contour is insulated (left) and at constant temperature (right).

these fluctuations, the standard deviations σ of the mean readings for different values of power input are estimated. Fig. 8 shows that the values of σ corresponding to the thermocouples located nearest the CC, at 0.207 and 0.230 m from the floor, show fluctuations five times greater than those registered in the other levels. The results also indicate that the fluctuations registered at 0.207 m are greater than those at 0.230 m, while all the others are uniform. Fig. 9 illustrates the variations of the mean standard deviation σ_P with respect to the power P. It is obtained averaging the standard deviations corresponding to the measurements of the thermocouples located between 0.046 and 0.180 m (red circles) and those located between 0.227 and 0.230 m (black squares). As observed, the intensity of the fluctuations diminishes when the power supplied by the heater increases, both in the fluid bulk and in the boundary layer near the upper contour.

The greatest fluctuations are detected where the strongest variations of the gradient occur according to synthetic schlieren results. As illustrated in Fig. 10, cyan zones corresponding to negative horizontal gradients appear alternating with light/dark blue zones of positive gradients below the upper boundary. The cyan zones resemble small plumes that separate from the top plate and consequently they must be composed of colder fluid. The locations of these plumes change with time randomly, and therefore a thermocouple registers an abrupt decrease of temperature when one of these plumes reaches it and an increase when the plume moves to another position, consistently with the fluctuations observed in Fig. 4b. Fig. 10 shows that these plumes of cold fluid reach a given height before they mix completely, thus suggesting the thickness of the boundary layer (between 0.184 and 0.207 m) in which the greatest variations of temperatures are registered. Significant spa-

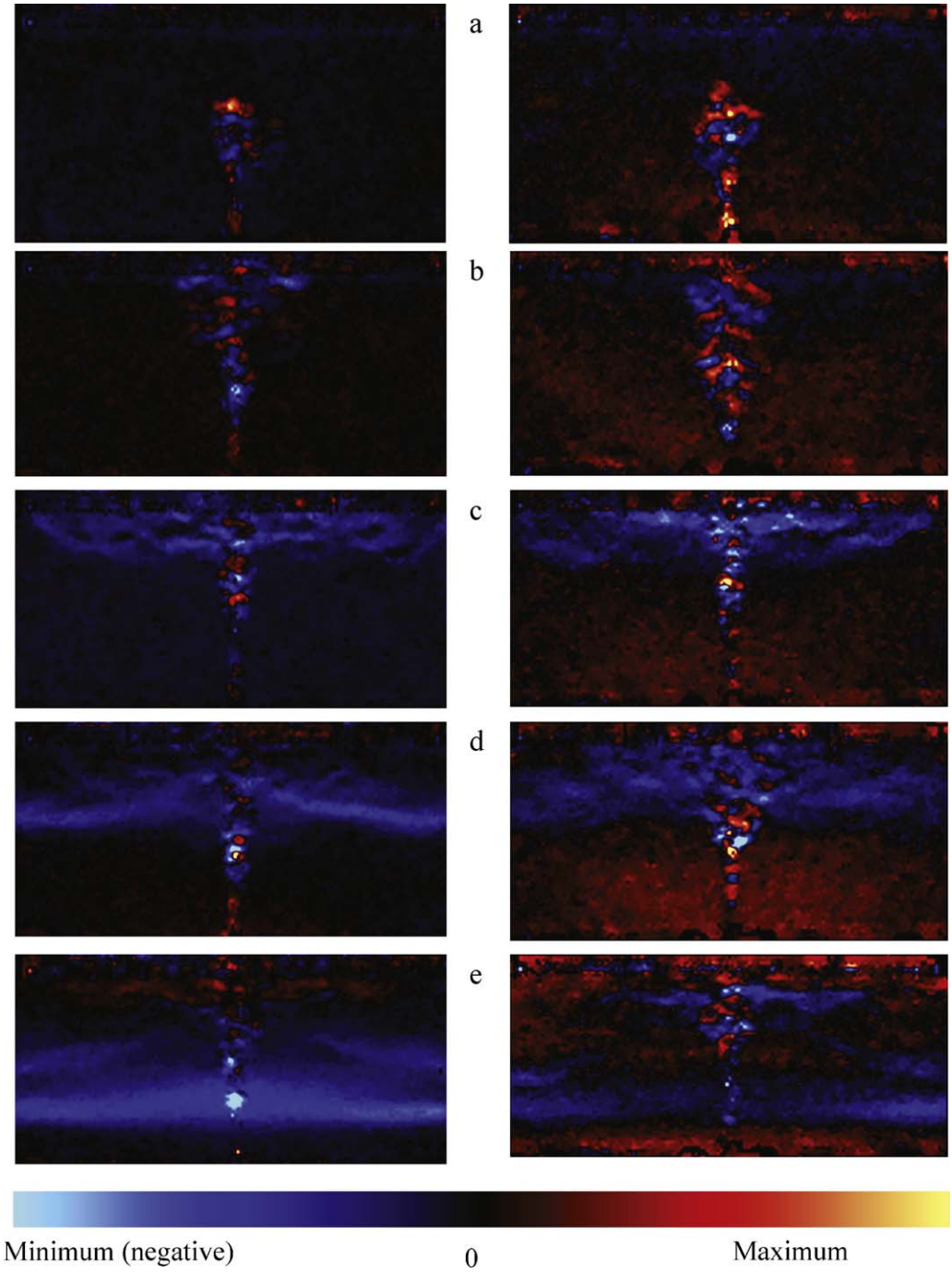

Fig. 3. Vertical component of the de temperature gradient corresponding to the same images shown in Fig. 2 for the insulated top box (left) and the cooled-ceiling system (right).

tial gradients are not observed in the fluid located below this layer, in agreement with the absence of important fluctuations in the results shown in Fig. 8.

The response in terms of frequency of the temperature measurements is another significant feature observed. The algorithm of the fast Fourier transform (FFT) was used to estimate the spectrum of frequencies that are multiples of the minimum frequency $(t_{end} - t_{initial})^{-1}$ up to the maximum value $(2dt)^{-1}$, where dt is the interval between measurements, and $t_{end} - t_{initial}$ is the processing interval, for different values of P and after the steady state regime is reached. Consistently with Figs. 9 and 10, the temperature fluctuations detected near the cooled top plate have greater amplitude than those in the fluid bulk. The frequency spectrum is similar in both cases and tends to a power law with a $-5/3$ exponent. No frequency has been found for which the amplitude is greater than the others, thus suggesting that there is no characteristic frequency in the measurement's range.

4. Analysis of the results

The CC system physically modeled here resembles the free convection in a fluid located between two heat conductor plates maintained at constant temperatures T_1 and T_2, with $\Delta T = T_1 - T_2 > 0$, known as Rayleigh–Benard (RB) convection. In RB

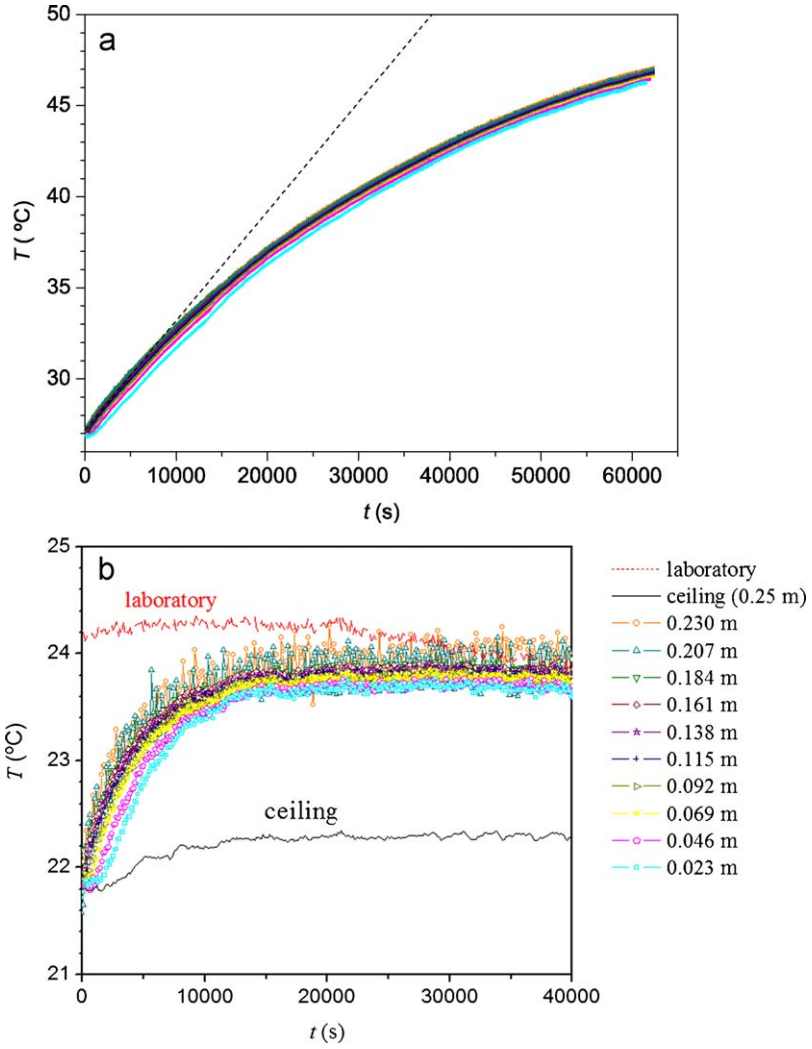

Fig. 4. (a) Evolution of the temperature at different height from the floor in the laboratory model with insulated top and a 60 W heater. The dashed line corresponds to the evolution of the expected mean temperature in a model without heat loses. (b) Evolution of the temperature at the cooled ceiling, ambient and at different heights in the fluid bulk for the experiments showed on the right of Figs. 2 and 3.

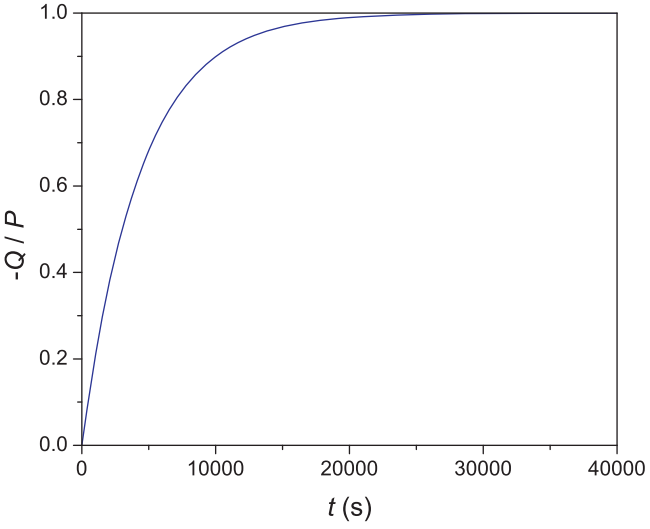

Fig. 5. Evolution of the heat flux Q at the upper contour for the CC case of Fig. 4b.

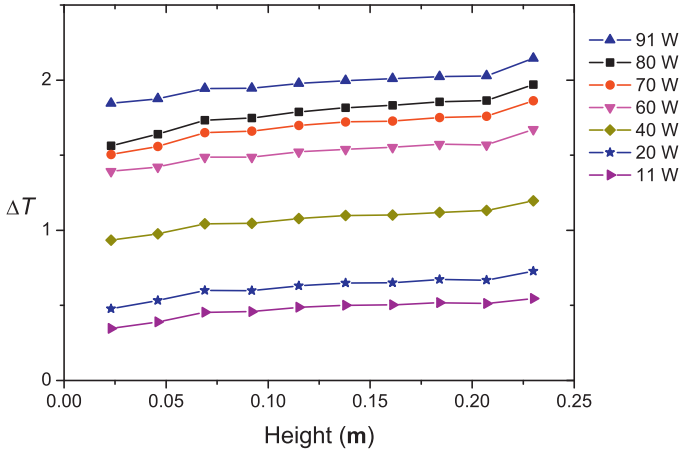

Fig. 6. Difference between the average $\langle T \rangle$ of the temperatures measured by the thermocouples immersed in the fluid at the height indicated in abscissas and the CC temperature T_{cc} during the steady state. The corresponding power values are indicated to the right of the figure.

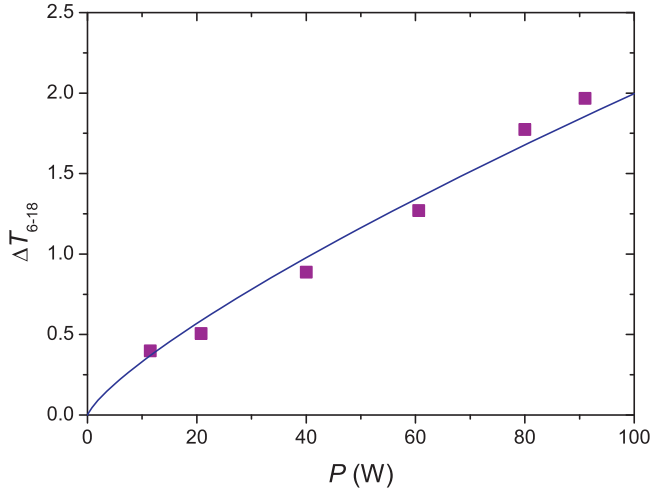

Fig. 7. Difference between the average of the temperatures measured with the thermocouples located between 0.069 and 0.184 m within the fluid, and T_{top} during the steady state regime. The line represents Eq. (7).

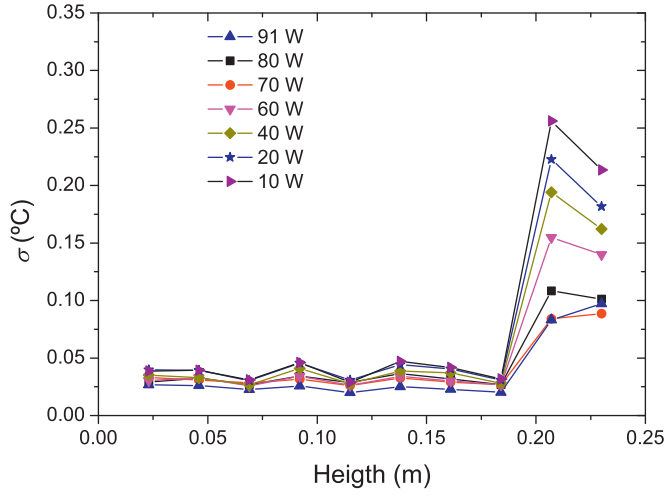

Fig. 8. Standard deviation σ of the time average of the temperature measurements shown in Fig. 4b.

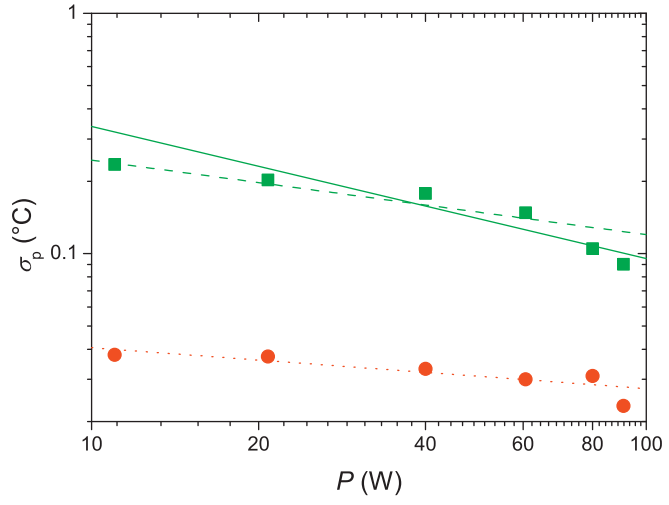

Fig. 9. Mean standard deviation as a function of the electric power. The straight lines correspond to power laws with exponents −0.55 (solid line), −0.31 (dashed line) and −0.17 (red dotted line). (For interpretation of the references to color in this figure legend, the reader is referred to the web version of the article.)

experiments, the heat flow in the fluid is characterized by the Rayleigh number

$$Ra = \frac{g\,\beta\,\Delta T\,L^3}{\nu\alpha}, \tag{1}$$

the ratio of the diffusivity properties of the fluid or Prandtl number

$$Pr = \frac{\nu}{\alpha} \tag{2}$$

and additional factors related to the shape and conditions of the contours that we name *bc*. In these equations g is the acceleration of gravity, L is the distance between plates and α, β and ν are the diffusivity, the thermal expansion coefficient and the kinematic viscosity (momentum diffusivity) of the fluid, respectively. The response of the system is often described as a function of the Nusselt number, or the relationship between the total heat flow and the heat flow by conduction

$$Nu = \frac{QL}{\lambda S\ \Delta T}, \tag{3}$$

and the Reynolds number

$$Re = \frac{LU}{\nu} = \sqrt{\frac{Ra}{Pr}} \tag{4}$$

where λ is the thermal conductivity, Q is the heat flux and S is the area of each plate. The velocity scale of the natural convection, $U = \sqrt{g\beta\,\Delta TL}$, suggest a characteristic frequency

$$f_c = \frac{U}{L} = \sqrt{\frac{g\beta\,\Delta T}{L}}. \tag{5}$$

As observed in Fig. 11, as *Ra* increases (for example, by increasing the temperature difference between the plates) the heat transfer also increases due to the increase of fluid velocity *U* and the change of the flow regime. For $Ra \gg 1$ we have $Nu \gg 1$, which indicates that the heat transfer by conduction is negligible according to (3).

The heat transfer driven by free convection is usually given by the relationship $Nu = Nu(Ra,Pr,bc)$ in the form

$$Nu = aRa^r Pr^p \quad \text{for} \quad Ra > 1700 \tag{6}$$

where the values of the coefficient a and exponents r and p vary according to the regime developed in the bulk of the fluid and in the boundary layers of the plates [23]. Here we adopt the values $a = 0.14$, $r = 0.29$, $p = 0$ as a first order approximation derived from different experimental and numerical results obtained using different fluids and represented in Fig. 11 with black symbols and lines, which was adapted from that reported by Itamoto et al. [24]. Naturally, for a limited range of *Ra*, the values of the parameters in (6) may be better fitted.

A variety of regimes (laminar, transient, oscillatory, steady, etc.) have been detected for different ranges of *Ra*, *Pr* and *bc*. The oscillatory regimes are usually associated with structures of the flow (big vortexes, for example) changing the sense or the position periodically with a frequency that may be estimated using (5). In these regimes the characteristic frequency and its multiples appear when the Fourier transforms of velocity and temperature are calculated; in addition the variations of those magnitudes in different points of the cell are correlated. When *Ra* is greater than a given characteristic value Ra^* ($\approx 10^6$ for water, for example), the convection becomes turbulent and the positions of the fluid elements fluctuate in a scale that is smaller than *L*. In such a case, the Reynolds number also increases for increasing ΔT according to (4) and the *U*-scale defined above.

The second column of Table 1 shows the main parameters involved in our problem estimated with Eqs. (1)–(5) as in a RB situation, which suggest that a completely developed turbulent regime is established. The green symbols (squares) in Fig. 11 represent

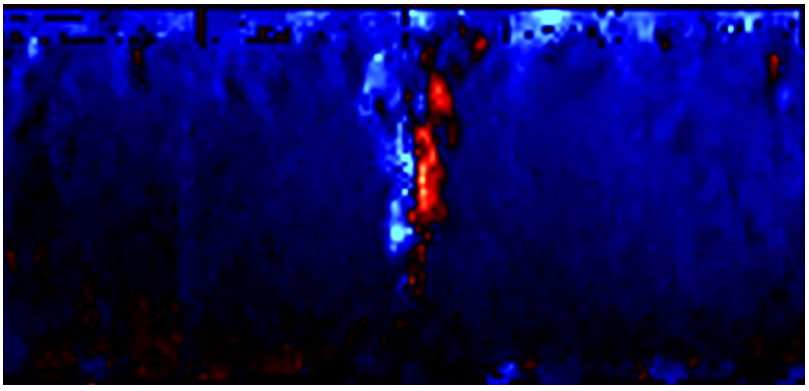

Fig. 10. Distribution of the horizontal component of the temperature gradient obtained by applying synthetic schlieren during the steady state.

Table 1
Main experimental parameters and their equivalent values in the RB experiments.

	Experimental values	RB equivalent values
L	0.25 m	0.50 m
Pr	6.4	6.4
ΔT	0.5–2 °C	1–4 °C
Ra	$(1–6)\times10^8$	$(2–10)\times10^8$
U	0.015–0.035 m/s	0.03–0.07 m/s
Re	$(0.4–0.9)\times10^4$	$(1.5–3.5)\times10^4$
Nu	95–160	95–160

$Nu = Nu(Ra)$ that drop far away from the general trend followed by the results obtained in the classical RB experiments. To explain this apparent disagreement we recall that a distinctive feature of the studied system is that the bottom plate is not at constant temperature as in RB experiments but has a heat source supplying a constant heat flux. Therefore, a useful comparison may be obtained if our experimental setup is considered as an RB experiment with plates separated a distance $2L$ and maintained with a temperature difference $2\Delta T$ as illustrated in Fig. 12. In this case the "equivalent" values shown in the third column of Table 1 are also determined and represented by the blue circles in Fig. 11. As seen, they are closer to the general trend, and fit better than those resulting from RB experiments.

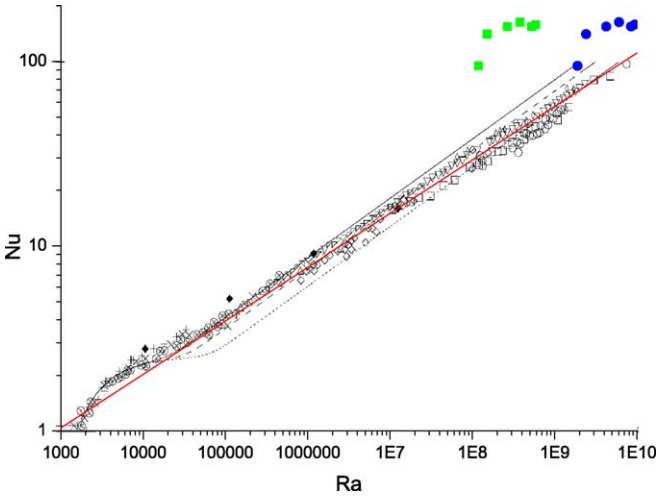

Fig. 11. Relationship between Nusselt and Rayleigh numbers found in RB experiments. Black points and best fit lines represent values and trends, respectively, obtained by other authors and reported by Itamoto et al. [24]. The solid red line is the approximation adopted in this work, while the green squares and blue circles correspond to our experiments. (For interpretation of the references to color in this figure legend, the reader is referred to the web version of the article.)

On the other hand, the power P supplied by the source is equal to the heat flux Q transferred during the steady-state regime. Since the energy entering the fluid is known, the parameters characterizing the final state are Nu, Pr and bc while the system adopts the necessary ΔT and Ra values for the fluid to transport the energy supplied by the source. Using Eqs. (1)–(3) and (6), it results that

$$\Delta T = \left[\left(\frac{L}{\lambda Sa}\right)\left(\frac{\nu\alpha}{g\beta L^3}\right)^r\left(\frac{\alpha}{\nu}\right)^p\right]^{1/1+r} P^{1/1+r}. \quad (7)$$

This relationship suggests that ΔT quasi-linearly depends on the source power because the values of r remain small, reasonably fitting the experimental points as shown in Fig. 7. An equation similar to (7) was proposed by Conroy and Mumma [25].

From RB experiments, it is also known that boundary layers with kinetic and thermal features (that is, boundary layers related to velocity U and energy transfer, respectively) form near the contours in which fluctuations of temperature and velocity are generated. Grossmann and Lohse [26] obtained scale laws for the fluctuations associated with the contributions of the background turbulence and with the plumes that separate from the contour. Thus, the amplitude T' of the temperature fluctuations is obtained as a Ra and Pr power law, consistently with the experimental results. Using Eq. (6), it is expressed $T' = f(Nu)$ as follows:

$$T' \sim Ra^q \sim Nu^{q/r}. \quad (8)$$

Particularly, for Pr = constant, the T' power law has an exponent $-0.11 < q < -0.16$ in agreement with the relative importance of both contributions. Castaing et al. [27] and Hayakawa and Tsuji [28] found a similar value of the exponent ($q \sim -0.14$) in the fluid bulk.

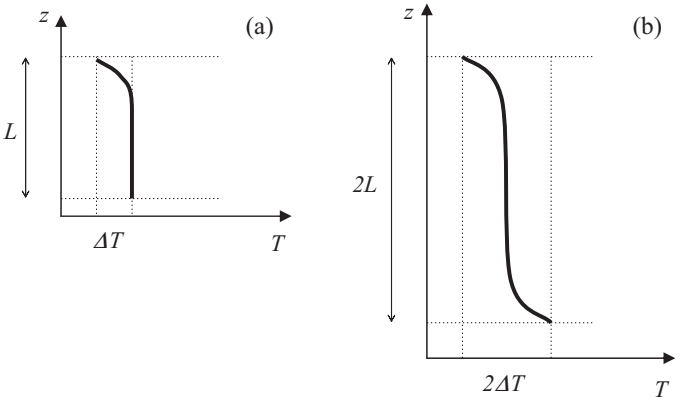

Fig. 12. The average temperature distributions corresponding to the experimental setup used here (a) and that of Rayleigh–Benard's (b).

According to this, the fluctuations below the cooled contour seem to be related to the fluctuations in the boundary layer and not to the turbulence in the fluid bulk. The Fourier transform does not show a special frequency of the order of the value indicated in Eq. (5) with amplitude notoriously greater than the others, while the energy spectrum is approximately proportional to $k^{-5/3}$. The latter is the power law in the inertial range of the spectrum when a homogeneous isotropic Kolmogorov turbulence is verified. This suggests that the turbulence is completely developed both in the fluid bulk and in the measurement points within the boundary layer, and that the chaotic motion of the fluid suppresses the formation of any coherent structures.

5. Conclusions

The convection generated by a heat source in the physical model of an insulated room with a top contour at a constant temperature (that is initially equal to the fluid bulk temperature) modeling a cooled-ceiling system is studied, and the features of the transient and steady states flows are described. The temperature evolution at specific height levels is obtained using an array of thermocouples and the temperature spatial variations are registered and quantified applying synthetic schlieren and digital image processing.

We observe that the initial dynamics of the flow is similar to that developed in the case of having an insulating ceiling (see for instance [14]). When the source is turned on, a plume forms and ascends with increasing velocity and the flow becomes turbulent. Once the plume reaches the top contour, the warm fluid spreads under it even when the ceiling maintains a constant temperature. Then a layer develops limited by a thermal front that descends progressively as in the filling-box case with the same velocity but smaller intensity. When the thermal front reaches the floor, the temperature of the fluid bulk and the heat flux Q absorbed by the cooled-ceiling increase almost uniformly with time. Finally the temperature of the bulk reaches a value a bit greater than that of the ceiling, achieving a steady state during which the heat supplied by the source is absorbed by the upper plate. Fluctuations of the temperature and spatial gradient variations with time suggest the presence of a boundary layer of about 0.05 m thick below the ceiling, where a flow different from that in the fluid bulk is developed. This layer is unstable because the temperature of the ceiling is smaller than that of the fluid bulk, which facilitates the formation of small plumes and vortexes that allow a more efficient heat transfer to the ceiling.

The relevant dimensionless numbers in the experiments are within the appropriate range to establish the dynamics similarity and then be compared to those characteristics of real situations [2]. This study helps to gain insight into the airflow in more complex situations as in family, commercial and industrial buildings. As an application, let us consider the next example: a 300 W-heat source is turned on in a 5.0 m-wide, 5.0 m-long and 2.5 m-tall closed room filled with air at 20 °C, and with a cooled-ceiling at the same temperature. We assume that the heat and air exchanges with adjacent rooms are negligible. In this case, the evolution described in Section 3.1 is fulfilled tending to a steady-state situation in which the mean temperature of the room increases by $\Delta T \approx 5$ °C according to Eq. (7). In the steady-state the velocity of the air circulation within the room is $U \approx 0.65$ m/s and the characteristic frequency associated with it (see Eq. (5)) allows the convective transfer of the heat supplied by the source to the cooled ceiling. Following the same reasoning used in Section 3.1, the cooled ceiling requires a time of the order of $\tau \approx 20$ min to start absorbing an important part of the heat supplied by the source. The time τ is much greater than the time given by the filling box model [1,2,14] because a non-negligible temperature difference is needed for the cooled ceiling to work as a heat drain. On the other hand, if the heat source is turned on for a smaller time than τ, the energy accumulates below the ceiling forming a stratified environment and finally the energy excess will be absorbed by the cooled ceiling, hardly affecting the people inside the room.

The results of the steady-state regime are explained using a correspondence with the classical RB experiments but considering a double separation between the floor and the ceiling for a similar temperature difference between the fluid bulk and the upper contour. However, some differences between the two cases compared deserve to be considered further. There not is a lower boundary layer and the characteristic distance L is included in the definition of the main parameters of the physical problem in a non-linear way ($Ra \sim L^3$, $Re \sim L^{3/2}$, $f_c \sim L^{-1/2}$). These features might produce different flow patterns, upper boundary layer structure and Nu from those corresponding situations in the RB experiments. Nevertheless, these differences seem to be minimal in the turbulent regime studied, although they might be more important for lower values of Ra and Re, with smaller or negligible turbulence. Also some kind of symmetrical flow may be originated for other locations of the source neither fixed nor symmetrical. These aspects deserve to be analyzed and are being considered in a new series of specific experiments.

Acknowledgements

This work was performed under the International Cooperation Project CONICET-CONACYT, the Project CONICET 054/2010 (Argentina) and the Project CONACYT 25116 (México).

References

[1] L.P. Thomas, B.M. Marino, R. Tovar, P.F. Linden, Buoyancy-driven flow between two rooms coupled by two openings at different levels, Journal of Fluid Mechanics 594 (2008) 425–443.
[2] P.F. Linden, The fluid mechanics of natural ventilation, Annual Review of Fluid Mechanics 31 (1999) 201–238.
[3] G.R. Hunt, P.F. Linden, The fluid mechanics of natural ventilation—displacement ventilation by buoyancy-driven flows assisted by wind, Building and Environment 34 (1999) 707–720.
[4] F. Alamdari, D.J.G. Butler, P.F. Grigg, M.R. Shaw, Chilled ceiling and displacement ventilation, Renewable Energy 15 (1998) 300–305.
[5] T. Runsheng, Y. Etzion, E. Erell, Experimental studies on a novel roof pond configuration for the cooling of buildings, Renewable Energy 28 (2003) 1513–1522.
[6] J. Dilip, Modeling of solar passive techniques for roof cooling in arid regions, Building and Environment 41 (2006) 277–287.
[7] J.L. Niu, L.Z. Zhang, H.G. Zuo, Energy savings potential of chilled-ceiling combined with desiccant cooling in hot and humid climates, Energy and Buildings 34 (2002) 487–549.
[8] J.-W. Jeong, S.A. Mumma, Practical cooling capacity estimation model for a suspended metal ceiling radiant cooling panel, Building and Environment 42 (2007) 3176–3185.
[9] R. Karadag, The investigation of relation between radiative and convective heat transfer coefficients at the ceiling in a cooled ceiling room, Energy Conversion and Management 50 (2009) 1–5.
[10] A. Novoselac, J. Srebric, A critical review on the performance and design of combined cooled ceiling and displacement ventilation systems, Energy and Buildings 34 (2002) 497–509.
[11] L. Juanico, A new design of roof-integrated water solar collector for domestic heating and cooling, Solar Energy 82 (2008) 481–492.
[12] H. Jiang, A. Okumura, A. Hoyano, K. Asano, A Solar cooling project for hot and humid climates, Solar Energy 71 (2001) 135–145.
[13] B.R. Morton, G.I. Taylor, J.S. Turner, Turbulent gravitational convection from maintained and instantaneous sources, Proceedings of the Royal Society A 234 (1956) 1–23.
[14] W.D. Baines, J.S. Turner, Turbulent buoyant convection from a source in a confined region, Journal of Fluid Mechanics 37 (1969) 51–80.
[15] G.R. Hunt, P. Cooper, P.F. Linden, Thermal stratification produced by plumes and jets in enclosed spaces, Building and Environment 36 (2001) 871–882.
[16] N.B. Kaye, G.R. Hunt, Time-dependent flows in an emptying filling box, Journal of Fluid Mechanics 520 (2004) 135–156.
[17] S.D. Fitzgerald, A.W. Woods, Transient natural ventilation of a space with localized heating, Building and Environment 45 (2010) 2778–2789.

[18] P.F. Linden, G.F. Lane-Serff, D. Smeed, A Emptying filling boxes: the fluid mechanics of natural ventilation, Journal of Fluid Mechanics 212 (1990) 300–335.
[19] N. Baker, P.F. Linden, Physical models of air flows: a new design tool, in: F. Mills (Ed.), Atrium Buildings Architecture and Engineering, CICC Publications, Welwyn, England, 1991, pp.13–22.
[20] A.V. Getling, Rayleigh–Bénard convection: Structures and Dynamics. Advanced Series in Nonlinear Dynamics, vol. 11, World Scientific Publishing, Singapore, 1998.
[21] S.B. Dalziel, G.O. Hughes, B.R. Sutherland, Whole-field density measurements by "synthetic schlieren", Experiments in Fluids 28 (2000) 322–335.
[22] S.B. Dalziel, DigiFlow User Guide, http://www.dalzielresearch.com.ar, 2010.
[23] G. Ahlers, S. Grossmann, D. Lohse, Heat transfer and large scale dynamics in turbulent Rayleigh–Benard convection, Reviews of Modern Physics 81 (2009) 503–537.
[24] I. Itamoto, H. Ishida, M. Higashiyama, D. Miki, G. Kawahara, Average and extremal properties of heat transfer and shear stress on a wall surface in Rayleigh–Benard convection, Heat and Mass Transfer 46 (2009) 153–165.
[25] C.L. Conroy, S.A. Mumma, Ceiling radiant cooling panels as a viable distributed parallel sensible cooling technology integrated with dedicated outdoor-air systems, ASHRAE Transactions 107 (1) (2001) 578–585.
[26] S. Grossmann, D. Lohse, Fluctuations in turbulent Rayleigh–Bénard convection: the role of plumes, Physics of Fluids 16 (2004) 4462–4472.
[27] B. Castaing, G. Gunaratne, F. Heslot, L. Kadanoff, A. Libchaber, S. Thomae, X.-Z. Wu, S. Zaleski, G. Zanetti, Scaling of hard thermal turbulence in Rayleigh–Benard convection, Journal of Fluid Mechanics 204 (1989) 1–30.
[28] T. Hayakawa, Y. Tsuji, Mean wind: its velocity and temperature fluctuation in low-Prandtl-number thermal convection, Physica D 239 (2010) 1353–1358.